# Exchange-biased magnetic tunnel junctions and application to nonvolatile magnetic random access memory (invited)

S. S. P. Parkin,[a] K. P. Roche, M. G. Samant, P. M. Rice, and R. B. Beyers
*IBM Research Division, Almaden Research Center, San Jose, California 95120*

R. E. Scheuerlein
*IBM Storage Division, San Jose, California 95120*

E. J. O'Sullivan, S. L. Brown, J. Bucchigano, D. W. Abraham, Yu Lu, M. Rooks, P. L. Trouilloud, R. A. Wanner, and W. J. Gallagher
*IBM T. J. Watson Research Center, Yorktown Heights, New York 10698*

Exchange biased magnetic tunnel junction (MTJ) structures are shown to have useful properties for forming magnetic memory storage elements in a novel cross-point architecture. MTJ elements have been developed which exhibit very large magnetoresistive (MR) values exceeding 40% at room temperature, with specific resistance values ranging down to as little as $\sim 60\ \Omega(\mu\text{m})^2$, and with MR values enhanced by moderate thermal treatments. Large MR values are observed in magnetic elements with areas as small as 0.17 $(\mu\text{m})^2$. The magnetic field dependent current–voltage characteristics of an MTJ element integrated with a silicon diode are analyzed to extract the MR properties of the MTJ element itself. © *1999 American Institute of Physics.* [S0021-8979(99)77508-0]

## I. INTRODUCTION

Recently there has been renewed interest in magnetic random access memory (MRAM) because of the development of novel highly magnetoresistive (MR) thin film magnetic structures, namely giant magnetoresistance (GMR) and the related spin-valve sandwich in metallic multilayered structures,[1] and magnetic tunnel junction (MTJ) structures.[2–6] MRAM possesses the attractive property of nonvolatility, namely the state of the memory is maintained even when power is removed from the memory. A variety of MRAM technologies have been explored over a period of many decades. Originally these involved macroscopic ferrite cores arranged in two- or three-dimensional arrays[7] but perhaps for the past 20 years or so interest has centered on magnetic thin film MRAM. Early interest centered on magnetic bubble technology involving the storage of information in continuous magnetic films[8] but this was not successful. In more recent years MRAM technologies have favored arrays of individually patterned magnetic storage cells or bits where one bit comprises a magnetic thin film multilayered structure. The magnetic bit is designed to have two stable magnetic states in zero and small magnetic fields which usually exhibit two different resistance values representing ''0'' and ''1''. Until recently such bits involved the use of the comparatively small anisotropic magnetoresistance (AMR) effect of conventional ferromagnetic materials arranged in thin film structures. While some of these structures are very ingenious,[9] these memories have been, not only of comparatively poor performance, but very expensive, and thus limited in their application.

Replacing AMR bit structures with GMR bit structures[10] has some obvious advantages. First the magnetic states of the GMR bit cells are much simpler. Second the larger GMR effects give rise to larger signals because of the higher MR values: the time required to read the state of the bit cell depends on how large is the difference in signal between the two states of the cell. Moreover the signal from a GMR cell in an appropriately designed MRAM can be sufficiently large that the bit may be read nondestructively without changing its magnetic state. This is not only faster still but consumes less power because the bit does not have to be subsequently rewritten.

Nevertheless even the larger signals available from GMR structures do not make GMR MRAM attractive for mainstream RAM applications. The reason for this is illustrated in Fig. 1(a). In order to achieve reasonable memory

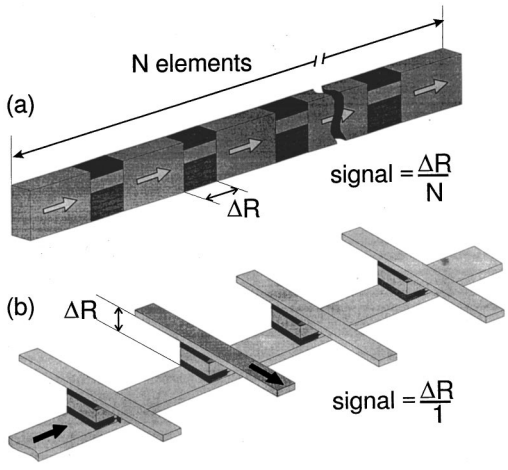


FIG. 1. Schematic illustration of (a) a number of GMR MRAM cells connected in series along a common bit line, and (b) a number of MTJ MRAM cells arranged along a common word line (lower line) at the cross points with corresponding upper bit lines.

[a]Electronic mail: parkin@almaden.ibm.com

 

array densities many GMR cells (of number $N$) have to be electrically connected in series which means that the actual signal available when reading one particular cell is $\sim$MR/$N$. This signal is not sufficient to make GMR MRAM competitive with conventional dynamic RAM (DRAM) and static RAM (SRAM).[11]

By contrast, as illustrated in Fig. 1(b), the high MR signal from individual MTJ storage cells can be fully utilized in a novel cross-point MRAM architecture,[12] by connecting each MTJ element in series to a switch, for example, a silicon diode. In this case, since current only passes through a single MTJ cell, the available signal when reading that cell is MR/1. With reasonable MR values such an MRAM architecture has the potential to rival that of DRAM in density, and SRAM in speed. In this article we address some of the materials issues required for making such a memory possible. We demonstrate useful MTJ structures, with areas as small as $0.2\times0.8\,(\mu\text{m})^2$, with very high MR values (>30%) at room temperature in small magnetic fields, and enhancement of these MR values on annealing at moderate temperatures. We also present MTJs with resistance–area products as low as $\sim$60 $\Omega(\mu\text{m})^2$ which will allow scaling of MTJ MRAM to densities needed for Gigabit memory chips. We show that the resistance and MR of MTJ elements in small test sites can be reasonably controlled and finally we demonstrate the operation of an MTJ integrated in series with a silicon diode.

## II. MAGNETIC TUNNEL JUNCTION MATERIALS

The basic magnetic tunnel junction comprises simply two ferromagnetic (FM) layers separated by a thin insulating tunnel barrier. The conductance of such sandwiches varies as the cosine of the angle between the magnetic moments of the two FM layers[13] and is highest when the magnetic moments are parallel to each other. The relative orientation of the magnetic moments in the most basic MTJ structures is varied by utilizing FM layers with different magnetic coercivities. Note that in lithographically patterned basic MTJ elements the magnetic switching fields of the FM layers can be readily varied by changing their self-demagnetizing fields, for example, by varying their shape or net magnetic moment. Nevertheless, it is useful to magnetically pin or magnetically harden one of the FM layers in an MTJ by exchange bias with an antiferromagnetic (AF) layer.[14] In contrast to exchange biased GMR sandwiches[15] the AF layer must be metallic because of an important difference between GMR and MTJ memory elements: namely, whereas in GMR elements the flow of sense current is parallel to the layers, in MTJ elements the current flows perpendicular to the layers.

Figure 2 shows a typical resistance versus field curve for a MTJ element with an area $A$ of $\sim40\times40\,(\mu\text{m})^2$, defined by metal contact masks. The structure is deposited by magnetron sputtering (3 mTorr argon, 1–2 Å/s deposition rate) at room temperature on a 0.5 $\mu$m thick $SiO_2$ layer on a 1 in. diam Si(100) wafer using, sequentially, three contact masks. The lower FM electrode consists first of a Ti/Pd seed layer, chosen both because it adheres well to $SiO_2$, and because it promotes the formation of $\gamma$-$Mn_{46}Fe_{54}$, an antiferromagnetic phase which is magnetically ordered well above room temperature. Next the first FM layer, 30 Å $Co_{84}Fe_{16}$, is deposited on top of the $\sim$100 Å thick MnFe layer. Then a thin metallic aluminum layer ($\sim$18 Å) is deposited through a second contact mask and subsequently plasma oxidized. Finally, a third contact mask is used to define the upper FM electrode which comprises 80 Å $Co_{84}Fe_{16}$/Pd/Ti. The complete structure is made *in situ* without breaking vacuum. The arrangement of the contact masks is shown as an insert to Fig. 2. Ten or more junctions are fabricated on each wafer and up to 20 wafers can be prepared in one pump-down of the vacuum chamber. The masks can be placed relative to one another within the vacuum chamber with an accuracy of $\sim$20 $\mu$m.

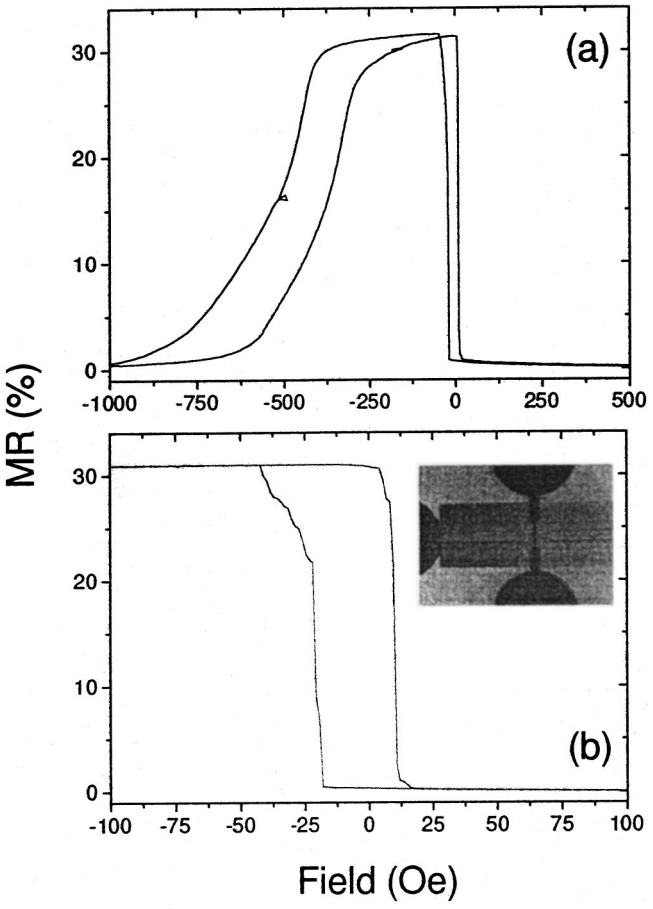


FIG. 2. Room temperature magnetoresistance vs field curves for a shadow masked MTJ structure with an area of $\sim40\times40\,(\mu\text{m})^2$. (a) shows the variation in resistance caused by the switching of the free FM layer close to zero field as well as the switching of the exchange biased FM layer at $\sim-500$ Oe. (b) shows the low field resistance curve in greater detail.

The MTJ in Fig. 2 has an MR$\sim$32% at room temperature and has a resistance $R\sim7\,\text{k}\Omega$, corresponding to a specific resistance $R_s=R\times A\sim11\,\text{M}\Omega(\mu\text{m})^2$. The reproducibility of MR and $R$ for the ten junctions on the same wafer is very good: MR and $R$ vary between $\sim$29% and $\sim$32% and $\sim$6.5 and $\sim$8 k$\Omega$, respectively. Larger MR values can readily be obtained by varying the composition of the CoFe layer with values of more than 42% at room temperature for $Co_{40}Fe_{60}$ layers.

Shadow masked junctions are very useful for rapidly exploring MTJ materials and structures but it is not possible to fabricate junctions with realistic dimensions for useful

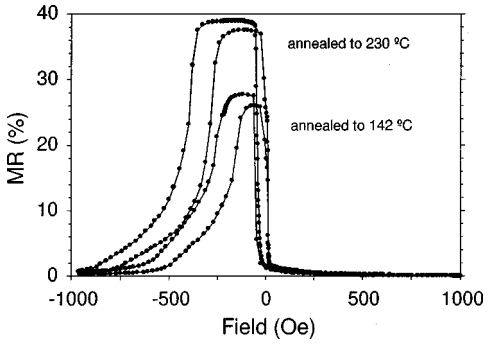


FIG. 3. Room temperature resistance vs field curve of a shadow masked MTJ structure after the structure was annealed initially at 140 °C and after a series of successive anneals at temperatures up to ~230 °C.

MRAM structures. Moreover our studies with shadow masks are limited to junctions with specific resistance values greater than $\sim 10^4\ \Omega(\mu\text{m})^2$ because for lower resistance values the current through the junction may not be uniform.[16,17] This can give rise to, for example, apparent decreased resistance and enhanced MR values. Indeed, under these circumstances, we have observed MR values as high as 1000%!

MTJ junctions with dimensions ranging from ~100 $\mu$m to submicrons were fabricated by the use of optical and *e*-beam lithography using a self-aligned process as described elsewhere.[6,18] The stability of MTJ structures to thermal treatments during such patterning, for example, during the baking of photoresists, is very important. It appears that the critical element of an MTJ structure, namely the Al–O tunnel barrier, is highly thermally stable. Moreover, contrary to GMR structures, the MR is typically increased by thermal treatments at moderate temperatures.[19] An example is given in Fig. 3 where the resistance versus field curves of an MTJ structure with an exchange-biased fixed Co layer and a $Ni_{40}Fe_{60}$ free or sense ferromagnetic layer are compared after thermal treatments at 140 °C (for setting the MnFe exchange bias) and after a series of thermal treatments up to 230 °C. In the latter case the sample was annealed successively at higher temperature temperatures in ~20 °C steps for 60 min intervals. The resistance of the junction was only weakly affected by the thermal treatment but the MR systematically increased for thermal treatments up to ~230 °C. After annealing at higher temperatures the MR of the structure decreased systematically although the resistance changed very little. We suppose that the increased MR is related to improvements in the tunnel barrier, either for example, by oxidation of any aluminum metal in the barrier by homogenization of the barrier or, more likely, by an improved interface with the lower FM electrode. The latter is consistent with a reduction, on thermal treatment, in a small amount of cobalt oxide observed in related test structures by x-ray absorption measurements. Increased MR values with thermal treatments were observed for a wide range of MTJ structures and materials.

## III. MAGNETIC TUNNEL JUNCTION MEMORY CELL PROPERTIES

In Fig. 1(b) a series of MTJ memory cells are shown at the cross points between a lower ''word'' line and an upper

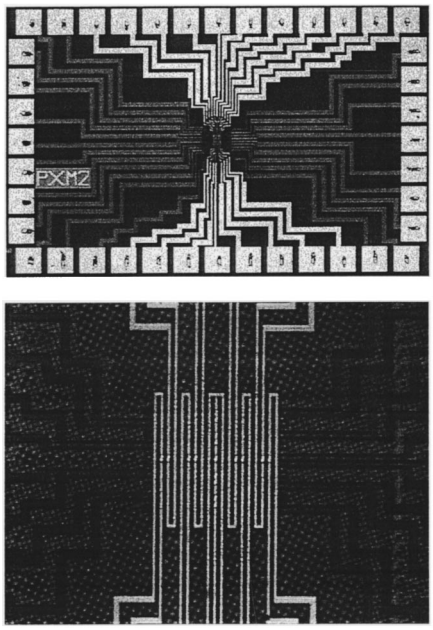


FIG. 4. Optical micrographs of an MTJ test site chiplet. The chiplet has 40 contact pads which can be seen in the upper micrograph. The lower micrograph is a high resolution image of the middle portion of the upper micrograph. The test site contains 17 MTJs, each $\sim 0.3\times 0.8\,(\mu\text{m})^2$ in size distributed along the central horizontal and vertical metallic contact electrodes (visible as brighter regions).

''bit'' line. These metal lines are conductors through which electrical current can be passed. Typically magnetic memories use a combination of orthogonal bit and word lines[7] in order to be able to individually address each magnetic memory cell to set or ''write'' its magnetic state. The vector combination of the orthogonal magnetic self-fields of the currents or current pulses passed through these lines is arranged such that the magnetic state of the selected memory element at the intersection of the chosen bit and word lines can be appropriately set. On the other hand the self-fields of these same currents must be such that the magnetic state of the half-selected devices along the same bit and word lines is not altered. Nevertheless these latter cells will be magnetically disturbed and it is very important that even after many such disturbances the magnetic state of these cells does not ''creep'' either to some intermediate state or completely reverse. Unpatterned MTJs without exchange-bias layers appear to be susceptible to creep.[20]

In order to explore such properties as well as to characterize the magnetic and transport properties of magnetic tunnel junctions on a size scale and pitch relevant to MRAM a test site shown in Fig. 4 was used. The upper part of Fig. 4 shows a low magnification micrograph of the test site showing 40 contact pads at the extremities of the chiplet. The test site consists of two levels of Al metallization in between which are sandwiched magnetic tunnel junctions. The bright areas in the high magnification image correspond to the top metal wiring which is at a pitch of 1.9 $\mu$m: 17 depressions can be seen indicating the locations of 17 MTJ devices which populate the array in cross pattern (i.e., the center vertical and horizontal lines). Two contact pads are used to contact each of the top and bottom electrodes so that four

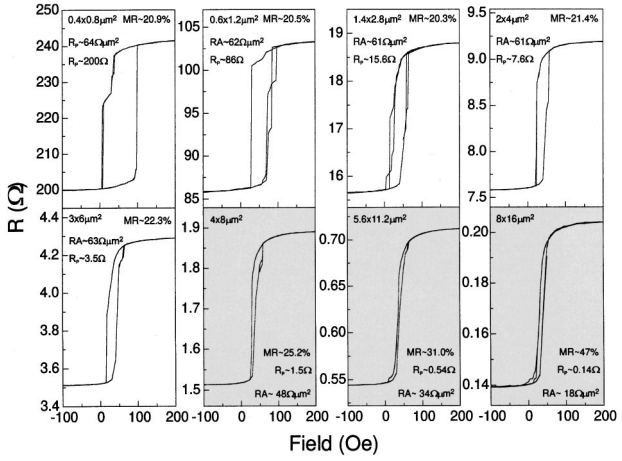


FIG. 5. Resistance vs field curves at room temperature of a series of related rectangularly shaped MTJs with sizes in $(\mu m)^2$, of $0.4\times0.8$, $0.6\times1.2$, $1.4\times2.8$, $2\times4$, $3\times6$, $4\times8$, $5.6\times11.2$, and $8\times16$. Each magnetic tunnel junction has the same structure as follows: bottom FM electrode: 50 Å Ta/250 Å Al/40 Å $Ni_{60}Fe_{40}$/100 Å $Mn_{54}Fe_{46}$/40 Å Co/7 Å Ru/30 Å Co/, tunnel barrier: 7 Å Al thermally oxidized, and, top electrode: 75 Å $Ni_{60}Fe_{40}$/250 Å Al/75 Å Ta. Note that the resistance and MR of the three largest junctions (shaded panels) are artificially decreased and increased, respectively, because of nonuniform current flow through these junctions.

point electrical measurements are possible on all 17 junctions. Underneath the bright metallic lines, the wires contacting the bottom electrode level can be seen, which are on a finer 0.8 $\mu$m pitch. The junctions in this particular array were approximately $0.3\times0.8\,(\mu m)^2$ in size and were defined using *e*-beam lithography. The cross pattern for the junctions allows for the study of interactions that might occur between nearest-neighbor junctions in the two orthogonal directions.

Figure 5 shows resistance versus field curves for a series of related MTJ structures patterned from a single wafer, each rectangular in shape and of the same aspect ratio, but with areas ranging from $0.4\times0.8\,(\mu m)^2$ to $8\times16\,(\mu m)^2$. The specific resistance of each of these junctions is $\sim60\ \Omega(\mu m)^2$ approximately 200 000 times lower than the specific resistance of the MTJs in Figs. 2 and 3. The lower resistance is obtained by the use of thinner Al layers $\sim7$ Å thick. The resistance of MTJs can be varied from $>10^9\ \Omega(\mu m)^2$ to as low as 60 $\Omega(\mu m)^2$ by varying the Al thickness and properly oxidizing it. As first discussed by Parkin *et al.*[5] incomplete oxidation leads to the presence of metallic Al in the barrier which results in a rapid suppression of the MTJ magnetoresistance. This result is in contradiction to the early claims of Moodera *et al.*[4] and Daughton *et al.*[21] that a thin unoxidized metallic layer of Al at the lower FM electrode interface with the tunnel barrier was essential to the observance of high MR values in MTJs. On the other hand overoxidation of the Al layer results in oxidation of the surface of the lower FM electrode which also results in diminished MR. While the Al layer can be oxidized by a multiplicity of different techniques each one must be optimized for each Al thickness.

The structure of the MTJs in Fig. 5 consists of a bottom FM electrode of the form: 50 Å Ta/250 Å Al/40 Å $Ni_{60}Fe_{40}$/100 Å $Mn_{54}Fe_{46}$/40 Å Co/7 Å Ru/30 Å Co/, a tunnel barrier of the form: 7 Å Al, and, a top electrode consisting of: 75 Å $Ni_{60}Fe_{40}$/250 Å Al/75 Å Ta. The 7 Å Al layer was oxidized by thermal or natural oxidation by exposing the layer to oxygen within the vacuum chamber. Note that the exchange biased FM layer comprises a Co/Ru/Co sandwich. The thin Ru layer strongly antiferromagnetically exchange couples the two Co layers so that their magnetic moments are arranged antiparallel to each other.[22,23] This provides greater stability to the pinned FM layer and additionally reduces the magnetostatic coupling of this layer to the free layer as well as to the FM layers of neighboring MTJ elements.[24] For this reason Fig. 5 only shows the switching of the free layer moment: the field required to switch the exchange biased layer is on the order of $\sim10$ kOe and outside the range of the experimental apparatus with which these measurements were made.

The data in Fig. 5 show that the resistance of the MTJ element scales inversely with the area of the MTJ element, whereas the MR of the element is essentially independent of the area of the device. Note that for the larger area devices in Fig. 5 the resistance values are artificially lowered and the MR values artificially raised presumably as a consequence of nonuniform current flow through these devices when the resistance of the tunnel barrier becomes comparable with the lateral in-plane resistance of the top or bottom electrodes.[16,17] Note also that the magnetic field required to switch the free layer increases systematically as the area of the MTJ devices is decreased as a result of the increased demagnetization field from the free layer magnetic moment. This field scales approximately inversely with the length of the device. The offset field of the free layer resistance versus field loop also increases as the size of the junction is decreased.[18] In all cases the offset field is consistent with an antiparallel coupling of the free and pinned FM layers as a consequence of the magnetostatic coupling between these layers which decreases with increased junction size.[25] In the limit of very large area junctions there is typically a residual ferromagnetic coupling between the free and pinned FM layers perhaps resulting from orange-peel coupling.[26]

Figure 6(a) shows a cross section transmission electron micrograph (XTEM) of an MTJ test site showing four MTJ cells sandwiched between an upper bit line and four word lines. The bit and word lines are formed from $Al_{96}Cu_4$. The MTJ devices are of area $\sim0.3\times0.8\ (\mu m)^2$: the MTJs have been sectioned along their shortest side. Figure 6(b) shows a higher magnification XTEM of one MTJ storage cell as well as a cartoon describing the structure of the MTJ cell. In order to avoid growing the MTJ directly on the top of the word line, which may be rough, and which would likely either be recessed beneath or protruding above the dielectric surrounding it, the MTJ is grown on a thin insulating $SiO_2$ layer which can be readily prepared very smoothly. This layer electrically isolates the MTJ from the word line. Since the lower electrode of the MTJ must be accessed electrically for reading purposes, a thin metallic lateral electrode, shown as the MX layer in the figure, extends to an adjacent via which contacts a lower metal region. (The connection to the word line is not visible in the XTEM.)

In a real memory device the MX layer would likely be connected by a via in a lower level to complementary metal–

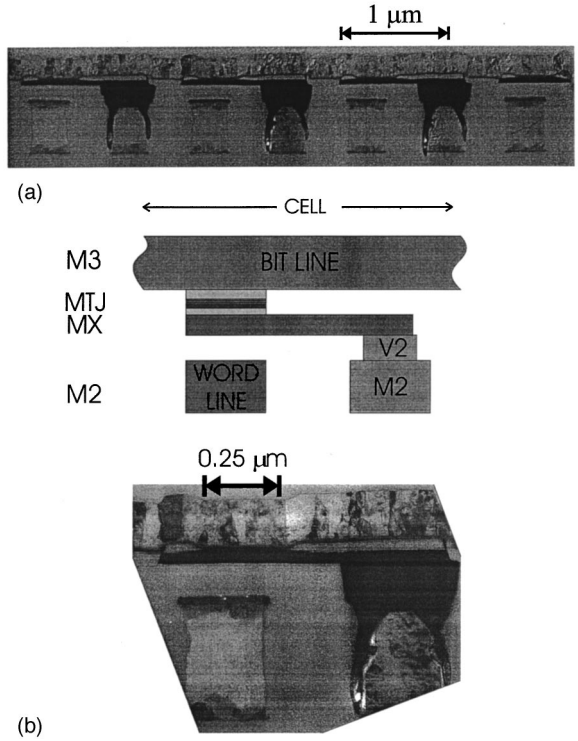


FIG. 6. Cross section transmission electron micrograph of an MTJ test site chiplet showing (a) a series of four neighboring MTJs and (b) a single MTJ cell illustrating the deposition of the MTJ on a $SiO_2$ layer above a word line. The cartoon describes the cross section.

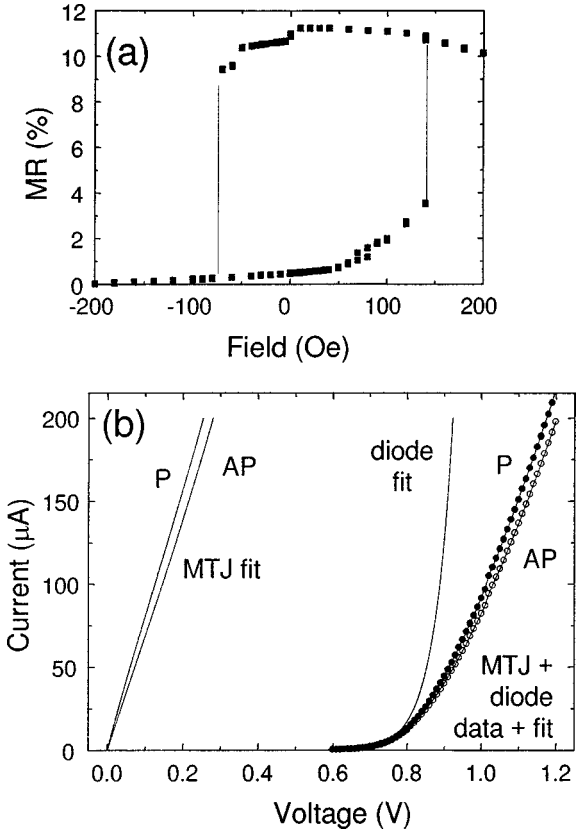


FIG. 7. (a) MR vs field curve of a compound device consisting of an MTJ integrated with a silicon diode at a bias voltage of 1 V. (b) Current vs voltage curves measured across the compound device in zero magnetic field with the MTJ in either its *P* or AP configuration. Fits to these curves are also shown including the extracted fitted $I-V$ curves corresponding to the diode and MTJ itself (in its *P* and AP states).

oxide–semiconductor (CMOS) circuits arranged in the silicon surface beneath it. In particular, this would allow the possibility of connecting, in series with each MTJ, a diode between the MTJ and its associated word line. This is an important feature of the MRAM cross-point architecture. The bit and word lines can be electrically biased so that only one diode is forward biased so that the sense current flows only through a single chosen MTJ device in the memory array.[11] In the absence of such a diode all the MTJs at each intersection of every bit and word line in the cross-point array would otherwise be electrically connected to one another. Note that for optimum performance, the resistance of the MTJ must be matched to that of the effective resistance of the diode. This can be achieved because of the large available range of $R \times A$ of the MTJ devices described above.

Figure 7(a) shows an example of a magnetoresistance versus field curve of such a compound device consisting of an MTJ integrated in series with a diode fabricated on the surface of a standard silicon wafer. The MTJ is nominally hexagonally shaped with outer dimensions of $\sim 0.3 \times 0.8\,(\mu\text{m})^2$ and a nominal area of $\sim 0.23\ (\mu\text{m})^2$. The loop was measured at a 1 V bias applied to the compound device. The shape of the MR curve is similar to that of otherwise identical MTJ devices on the same wafer but without the diodes connected. The current–voltage ($I-V$) characteristics of this compound device were measured at zero field after saturating the junction in positive and negative fields so as to set the MTJ in its two remanent magnetic states with the FM layers either parallel (*P*) or antiparallel (AP) to each other. To separate the diode characteristics from the MTJ characteristics, the $I-V$ curves corresponding to the *P* and AP states were fitted to a model for a standard diode in series with a nonlinear resistor. The same diode parameters were used for both curves, with different linear plus cubic terms used to describe the two MTJ characteristics. Figure 7(b) shows the measured data for the two zero-field $I-V$ curves and the very good fit to these two curves. The model curves for the diode by itself and the MTJ by itself for the two remanent states (*P* and AP) are also shown. From these fits, the resistance of the MTJ itself as a function of voltage on the junction can be extracted. This fit gives an MR value at low bias voltage of $\sim 17\%$, which is consistent with the MR values measured directly on isolated MTJs on the same wafer.

Finally, Fig. 8 shows resistance versus field curves for two sets of 14 nominally identical junctions measured in a MRAM test chiplet similar to that shown in Fig. 4 except that the wires are $\sim 4\ \mu$m wide on a 8 $\mu$m pitch. The junctions have nominal dimensions of $2 \times 4$ and $0.6 \times 1.2\,(\mu\text{m})^2$ in Figs. 8(a) and 8(b), respectively. The easy axes of the junctions are along their longer axis in both cases. The structure of these junctions is identical to that of those in Fig. 5 except that the thickness of the $Ni_{60}Fe_{40}$ free FM layer is reduced to 50 Å in (b) and the Al thickness is increased to $\sim 9$ and $\sim 11$ Å in (a) and (b), respectively. The

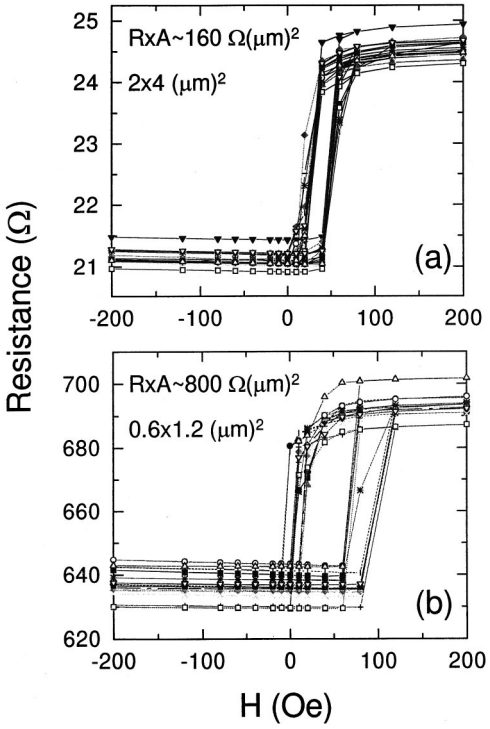


FIG. 8. Resistance vs field curves of two sets of 14 nominally identical MTJ devices measured in a test-site chiplet similar to that of Fig. 4. The structures are similar to those of Fig. 5 but with Al layer thicknesses of (a) 9 Å and (b) 11 Å.

junctions have corresponding $R \times A$ values of $\sim$150 and 800 $\Omega(\mu m)^2$, respectively. Figure 8 shows that, notwithstanding the large dependence of junction resistance on Al thickness, the local uniformity of the junction resistance and MR is very good. Indeed the variation in resistance and MR from junction to junction is less than $\pm 1.5\%$ for both sets of junctions. As can be seen from Fig. 8 the variation in magnetic switching field from junction to junction is much larger. Note that the switching fields are much larger in the smaller junctions in Fig. 8(b) because of the larger demagnetizing fields. The large variation in switching field is most likely attributable to small defects in the definition of the shape of the MTJ elements.

## IV. CONCLUSION

We have developed MTJ devices that exhibit more than 40% MR at room temperature in small magnetic fields. In addition, we have shown that the resistance of such MTJ devices can be varied over a very wide range. This makes it possible to impedance match such MTJ memory elements with required semiconductor solid-state circuit devices even for very dense memories of gigabit and greater sizes. We have demonstrated the possibility of accessing a MTJ device using a silicon diode integrated in series with the device. Using specially designed MRAM test sites we have demonstrated excellent local uniformity of MTJ resistance and MR but poorer control of magnetic switching fields. In summary we have established that exchange biased magnetic tunnel junction devices form attractive candidates for magnetic nonvolatile storage elements.

## ACKNOWLEDGMENTS

This study was partly supported by DARPA under Contract No. MDA972-96-C-0030. The authors thank T. Donahue, T. Furakawa, Y. Lee, K.-S. Moon, A. C. Marley, K. Pettit, and John Connolly for useful discussions and help. They also thank J. Stohr for x-ray absorption measurements.

[1] S. S. P. Parkin, in *Annual Review of Materials Science*, edited by B. W. Wessels (Annual Reviews Inc., Palo Alto, CA, 1995), Vol. 25, pp. 357–388.
[2] M. Julliére, Phys. Lett. **54A**, 225 (1975).
[3] T. Miyazaki and N. Tezuka, J. Magn. Magn. Mater. **139**, L231 (1995).
[4] J. S. Moodera, L. R. Kinder, T. M. Wong, and R. Meservey, Phys. Rev. Lett. **74**, 3273 (1995).
[5] S. S. P. Parkin, R. E. Fontana, and A. C. Marley, J. Appl. Phys. **81**, 5521 (1997).
[6] W. J. Gallagher, S. S. P. Parkin, Y. Lu, X. P. Bian, A. Marley, K. P. Roche, R. A. Altman, S. A. Rishton, C. Jahnes, T. M. Shaw, and G. Xiao, J. Appl. Phys. **81**, 3741 (1997).
[7] R. E. Matick, *Computer Storage Systems and Technology* (Wiley, New York, 1977).
[8] A. H. Eschenfelder, *Magnetic Bubble Technology* (Springer, Berlin, 1980), Vol. 14.
[9] J. M. Daughton, Thin Solid Films **216**, 162 (1992).
[10] D. D. Tang, P. K. Wang, V. S. Speriosu, S. Le, and K. K. Kung, IEEE Trans. Magn. **31**, 3206 (1995).
[11] R. E. Scheuerlein, Proc. IEEE International Nonvolatile Memory Technology Conference, Albuquerque, NM, 22–24 June 1998.
[12] W. J. Gallagher, S. S. P. Parkin, R. E. Scheuerlein, and J. Kaufman, US Patent and Trademark Office, Patent No. 5,640,343 (1997).
[13] J. C. Slonczewski, Phys. Rev. B **39**, 6995 (1989).
[14] A. Yelon, in *Physics of Thin Films: Advances in Research and Development*, edited by M. Francombe and R. Hoffman (Academic, New York, 1971), Vol. 6, p. 205.
[15] S. S. P. Parkin, Phys. Rev. Lett. **71**, 1641 (1993).
[16] R. J. Pedersen and F. L. Vernon, Appl. Phys. Lett. **10**, 29 (1967).
[17] J. S. Moodera, L. R. Kinder, J. Nowak, P. LeClair, and R. Merservey, Appl. Phys. Lett. **69**, 708 (1996).
[18] Y. Lu, R. A. Altman, A. Marley, S. A. Rishton, P. L. Trouilloud, G. Xiao, W. J. Gallagher, and S. S. P. Parkin, Appl. Phys. Lett. **70**, 2610 (1997).
[19] S. S. P. Parkin *et al.* (unpublished).
[20] S. Gider, B.-U. Runge, A. C. Marley, and S. S. P. Parkin, Science **281**, 797 (1998).
[21] J. M. Daughton, J. Appl. Phys. **81**, 3758 (1997).
[22] S. S. P. Parkin, N. More, and K. P. Roche, Phys. Rev. Lett. **64**, 2304 (1990).
[23] S. S. P. Parkin and D. Mauri, Phys. Rev. B **44**, 7131 (1991).
[24] S. S. P. Parkin and D. E. Heim, US Patent and Trademark Office, Patent No. 5,465,185 (1995).
[25] K.-S. Moon, R. E. Fontana, and S. S. P. Parkin (unpublished).
[26] L. Néel, Ann. Phys. (Leipzig) **2**, 61 (1967).